RSC Advances

ROYAL SOCIETY OF CHEMISTRY

www.rsc.org/advances

Photocatalytic activity of Ag nanoparticles-dispersed N-TiO_2 nanofilms by magnetron sputtering

Wanggang Zhang [1,2], Yiming Liu [1,2], Diaoyu Zhou[1,2], Jing Wen[1,2], Wei Liang[1,2,*], Fuqian Yang[1,2,3,*]

[1] College of Materials Science and Engineering, Taiyuan University of Technology, Taiyuan Shanxi 030024, China

[2] Key Laboratory of Interface Science and Engineering in Advanced Materials, Taiyuan University of Technology, Ministry of Education, Taiyuan Shanxi 030024, China

[3] Department of Chemical and Materials Engineering, University of Kentucky, Lexington, KY 40506, USA

Table of contents entry

Back-scattered electron image and secondary electron image of a scraped Ag 50nm/N-TiO_2 nanofilm after the heat treatment at 400 ^oC. Dependence of the degradation rate of the TiO_2-based nanofilms on the number of cycles for the photodegradation of MB. The degradation rate of the TiO_2-based nanofilms decreases with the number of cycles.

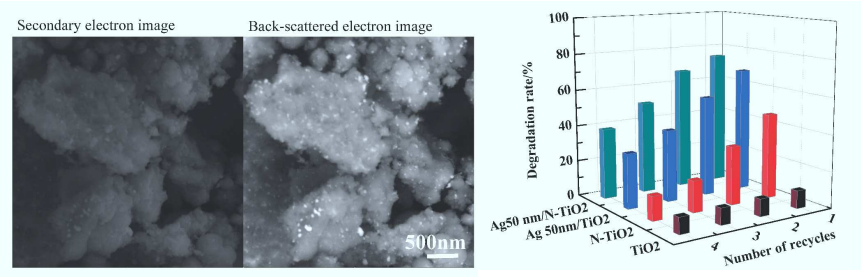

Corresponding author: Wei Liang, Email: liangwei@tyut.edu.cn;
Fuqian Yang, Email: fyang2@uky.edu.

Abstract

Using magnetron sputtering, pure TiO_2 nanofilms and Ag/TiO_2 bilayer nanofilms with N were deposited on glass substrates. Heat-treatment of the $Ag/N\text{-}TiO_2$ nanofilms at 400 ^oC led to the formation of Ag nanoparticles, which were dispersed inside the TiO_2 films as well as on the free surface of the TiO_2 films. The photocatalytic activity of the $Ag/N\text{-}TiO_2$ nanofilms with the dispersion of Ag nanoparticles was examined by UV-vis diffuse reflectance spectroscopy. The rate constants for the photodegradation of methylene blue (MB) in the aqueous solutions of MB with $N\text{-}TiO_2$-based nanofilms are about one order larger than that of self-degradation and that with only pure TiO_2 nanofilms. The rate constants for the photodegradation of the aqueous solutions of MB with the $Ag/N\text{-}TiO_2$ nanofilms are larger than that with the $N\text{-}TiO_2$ nanofilms. The Ag nanoparticles improve the photocatalytic activity of TiO_2 films possibly through the surface plasmon absorption effect of Ag nanoparticles which activates photo-generated charge carriers through the transfer of plasmonic energy.

Keywords: magnetron sputtering; Ag, $N\text{-}TiO_2$; visible light; photocatalytic.

1. Introduction

TiO_2-based nanostructures have potential in various applications, including photocatalytic processes [1-4], lithium-ion batteries [5-8], solar cells [9-11], and supercapacitors [12]. In the heart of the photocatalytic processes of TiO_2-based nanostructures is the activity that leads to the formation of the photo-induced electron-hole pairs to activate a series of chemical reactions, resulting in the mineralization of pollutants [13, 14]. However, the fast recombination of the photogenerated electron–hole pairs [15], large optical-band gap (3.2 eV for anatase and 3.0 eV for rutile) [16], low electron mobility [17] and small diffusion length of minority carrier (hole) (10-100 nm) [18, 19] have limited the applications of TiO_2.

To increase the potential applications of TiO_2-based nanostructures, various methods, including the doping of non-metallic or metallic elements [20-23], have been developed to extend the work spectrum of TiO_2 to the visible (VIS) and infrared (IR) regions and to enhance the electron–hole separation. Noble metal nanoparticles, such as gold (Au) and silver (Ag) have been used to improve the photocatalytic efficiency under visible light irradiation. Kannaiyan et al. [24] used amphiphilic poly(styrene-block-ethylene oxide) diblock copolymer (PS-b-PEO) micelles loaded with $AgNO_3$ and TiO_2 sol–gel precursors as templates to fabricate hybrid Ag/TiO_2 nanodot arrays and observed that the Ag/TiO_2 nanodot arrays significantly increased photocatalytic degradation of methylene blue (MB) in comparison to pure TiO_2 nanoparticle arrays. Xu et al. [25] found the enhancement of the light absorption of the TiO_2/SiO_2 bilayer with the implantation of Ag nanoparticles in SiO_2 layer in comparison to TiO_2 films, which is likely due to the plasmonic effect near the interface of TiO_2 and silica glass.

The TiO_2-based composites with the doping of nitrogen have been intensively studied. Yang et al. [26] investigated the photocatalytic activity and stability of N-doped anatase TiO_2, using the decomposition of MB and methyl orange (MO) as model reactions under visible light irradiation, and showed that nitrogen has a significant effect on the optical absorption of TiO_2. They suggested that both the degree of N doping and oxygen vacancies contribute to the visible light absorption of the N-doped TiO_2 materials. Li et al. [21] showed the good photocatalytic activity and high stability of hierarchical N-doped TiO_2 microspheres with

exposed (001) facets [N-TiO_2-(001)] under visible light irradiation in comparison to the commercially available P25 TiO_2. Such a good photocatalytic activity for N-doped TiO_2 is likely due to the formation of intermediate energy levels in the band gap from either the mixing of N 2p with O 2p states or the presence of localized states [27, 28].

Currently, the preparation of doped TiO_2 structures has mainly based on solution-based techniques. There are various issues needed to be improved, including reproducibility, impurities, and removal of residuals. To fully utilize the good photocatalytic activity of N-doped TiO_2 structures and limit the concerns involving the use of the solution-based techniques, different techniques need to be developed to prepare N-doped TiO_2 structures. It is known that sputtering a metal of high purity on the surface of a substrate can lead to the formation of nanoparticles under certain conditions. This work explores the possibility of preparing N-doped TiO_2 nanofilms with the dispersion of Ag nanoparticles, using the magnetron sputtering technique. This approach offers several advantages over the solution-based techniques, including scalability, high purity, accurate control of metal loading, and solution-free synthesis. It limits the use of a reducing agent like sodium borohydride, washing treatment to remove residuals, or a high temperature reduction treatment. The characterization of the microstructures of the prepared N-doped TiO_2 nanofilms is performed by scanning electron microscopy (SEM), transmission electron microscopy (TEM) and X-ray diffraction (XRD). The photocatalytic activity of the prepared N-doped TiO_2 nanofilms is investigated by measuring the degradation behavior of the MB organic compound.

2. Experimental detail

Preparation of thin films

Ag nanofilms on glass substrates were prepared at room temperature (25 ^oC) by magnetron sputtering in a multifunctional magnetron sputtering instrument (JGP560B) under the condition of high vacuum, using an Ag target. Prior to sputtering, the glass substrates (2×2 cm^2) were ultrasonically cleaned with acetone, ethyl alcohol, and deionized water for 15 min, respectively. Argon gas was flowed into the sputtering chamber after the pressure of the sputtering chamber reached 8×10^{-4} Pa. Pre-sputtering of 3 min was performed to remove surface residuals. During the sputtering, the flow rate of argon gas was 30 sccm, and the

chamber pressure was 6 Pa. The distance between the glass substrate and the target was 30 mm, and the thicknesses of Ag nanofilms were controlled by the sputtering time.

After the deposition of Ag nanofilms, both argon gas and nitrogen gas were flowed simultaneously into the sputtering chamber to prepare N-doped TiO_2 nanofilms after the pressure of the sputtering chamber reached 8×10^{-4} Pa. The volume ratio of Ar to N_2 was 1:1, and the flow rate of individual gas was 15 sccm. The Ag/TiO_2 nanofilms without nitrogen were also prepared, using a similar approach. The prepared nanofilms were heat-treated at 400 ^{o}C for 3 h at a ramping rate of 2 ^{o}C·min^{-1} in a tube furnace in air.

Materials characterization

The surface topology of the prepared nanofilms was examined, using a Field Emission Scanning Electron Microscopy (FESEM) (Tescan MIRA 3 LMH) at 10 kV; the composition of the nanofilms was determined, using Energy Dispersive Spectroscopy (EDS) (OXFORD X-Max 20). The crystal structures of the nanofilms were analyzed with the Cu Kα line on a Rigaku D/max 2500 X-ray diffractometer (XRD) with patterns recorded in a range of 20°-80°. Optical absorption of the nanofilms in the wavelength range of 300-800 nm was measured, using a UV-vis spectrophotometer (HITACHI: U-3900). The banding energy was determined, using X-ray photoelectron spectroscopy (XPS) (Escalab 250).

Characterization of photocatalytic activity

The photocatalytic activity of the prepared TiO_2-based nanofilms was evaluated by measuring the degradation behavior of the MB organic compound in an aqueous solution under visible light irradiation. The aqueous MB solution (5 mg·L^{-1}) of 50 ml was placed in a shallow, round glass vessel with a diameter of 4.5 cm and stirred in the dark at room temperature for 30 min. 3 rectangular pieces of 20×20 mm^2 glass slide with the nanofilms were placed in the vessel, which was adequate under the experimental conditions without disturbing the visible light entering the glass vessel. The glass vessel was placed in an ice bath to maintain a constant temperature during characterizing the photocatalytic activity. A 300 W tungsten lamp (Philips Halogen) with a cutoff filter ($\lambda \geqq 420$ nm) at a distance of 20 cm above the solution was used to irradiate the aqueous MB solutions. The adsorption of MB on the surface of the TiO_2 nanofilms led to the decrease of the MB concentration in the

aqueous solution and the change of the absorbance of the MB aqueous solutions under visible light irradiation. To eliminate the effect of background, the photo-induced reactions were performed after mixing the TiO_2 nanofilms with the MB solution in the dark for half an hour to reach a steady state. All the samples for the experiment of photocatalytic activity were calcined at 400 ^oC.

It is known that visible light irradiation can cause the reduction of the cationic form of MB and the color change from blue to colorless through accepting photo-catalytically generated electrons [29]. The photo-induced MB degradation was thus determined from the absorbance of the MB peak at a wavelength of 664 nm, using an UV/vis spectrophotometer (Perkin-Elmer, Lambda 35), from which the MB concentration, c, was estimated as,

$$c = A_0 / A \quad (1)$$

where A_0 is the absorbance of MB at the beginning of the visible light irradiation, and A is the absorbance of MB at time t. The rate constant, k, is calculated as,

$$\ln(c_0 / c) = \ln(A / A_0) = kt \quad (2)$$

where c_0 is the concentration of the MB solution without visible light irradiation.

3. Results and discussion

X-ray diffraction analysis

X-ray diffraction (XRD) was carried out on Ag/N-TiO_2 nanofilms with the Ag film thicknesses of 20, 50, 80 nm, which are referred as Ag 20nm/N-TiO_2, Ag 50nm/N-TiO_2 and Ag 80nm/N-TiO_2, respectively. Figure 1 shows the XRD patterns of the Ag/N-TiO_2 nanofilms calcined at 400 ^oC. All the nanofilms clearly display the peaks of TiO_2, including the planes of (101), (004), (200), (204), and (220), at 2θ values of ca 25.3, 37.8, 48.1, 62.8, and 68.7^o, respectively. This result suggests that there is only the anatase phase in the Ag/N-TiO_2 nanofilms calcined at 400 ^oC.

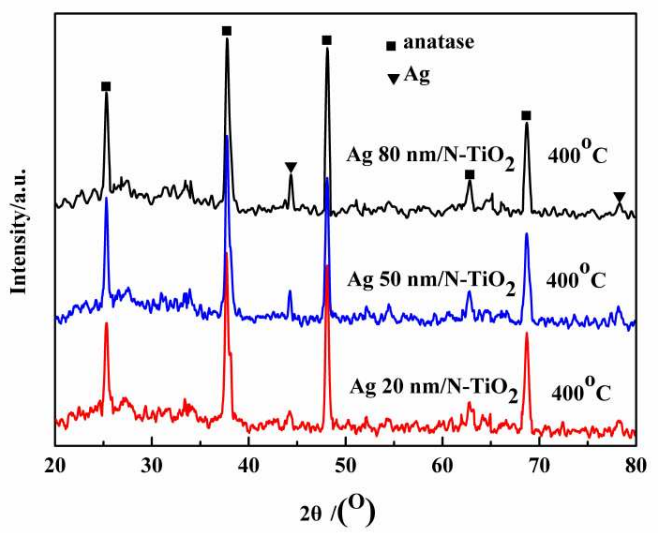

Figure 1. XRD patterns of Ag/N-TiO_2 nanofilms calcined at 400 °C

The peaks at 44.3 and 77.4° of the 2θ values are associated with the (200) and (311) diffractions of the cubic phase of Ag with a lattice constant of 4.0861 Å. This result suggests that Ag was present in the Ag/N-TiO_2 nanofilms. The peaks at 38.2 and 64.5° of the 2θ values of face-centered cubic Ag overlap the diffraction peaks of (004) and (204) at 37.8 and 62.6° of the 2θ values of TiO_2, respectively. It is difficult to detect the (111) and (204) planes of Ag from the XRD diffraction spectrum.

XPS analysis

The chemical state of Ag in the Ag/N-TiO_2 nanofilms was characterized by XPS. Figure 2a shows the Ag 3d fine XPS spectra of Ag/N-TiO_2 nanofilms. The binding energies for Ag $3d_{5/2}$ and Ag $3d_{3/2}$ levels are found to ca. 367.5 and 373.5 eV, respectively, which suggest that the state of Ag is metal Ag(0) [30, 31] and no silver oxide is present. Such a result is further supported by the O 1s spectra (Figure 2b), in which no new peaks appear except the peaks at ca. 529.6 and 531.4 eV. The peak at ca. 529.6 eV is ascribed to the Ti-O bonds in the TiO_2 lattice, and the peak at ca. 531.4 eV is related to the oxygen in the surface hydroxyl groups (H-O bonds) [32, 33]. It is evident that the peaks of Ag 3d shift to the lower positions in comparison to 368.3 eV for Ag $3d_{5/2}$ and 374.3 eV for Ag $3d_{3/2}$ of bulk Ag [34], which suggests

the migration of electrons from TiO_2 nanofilms to metallic Ag and a strong interaction between Ag nanostructures and TiO_2 nanofilms at the interface of the nano-heterostructures.

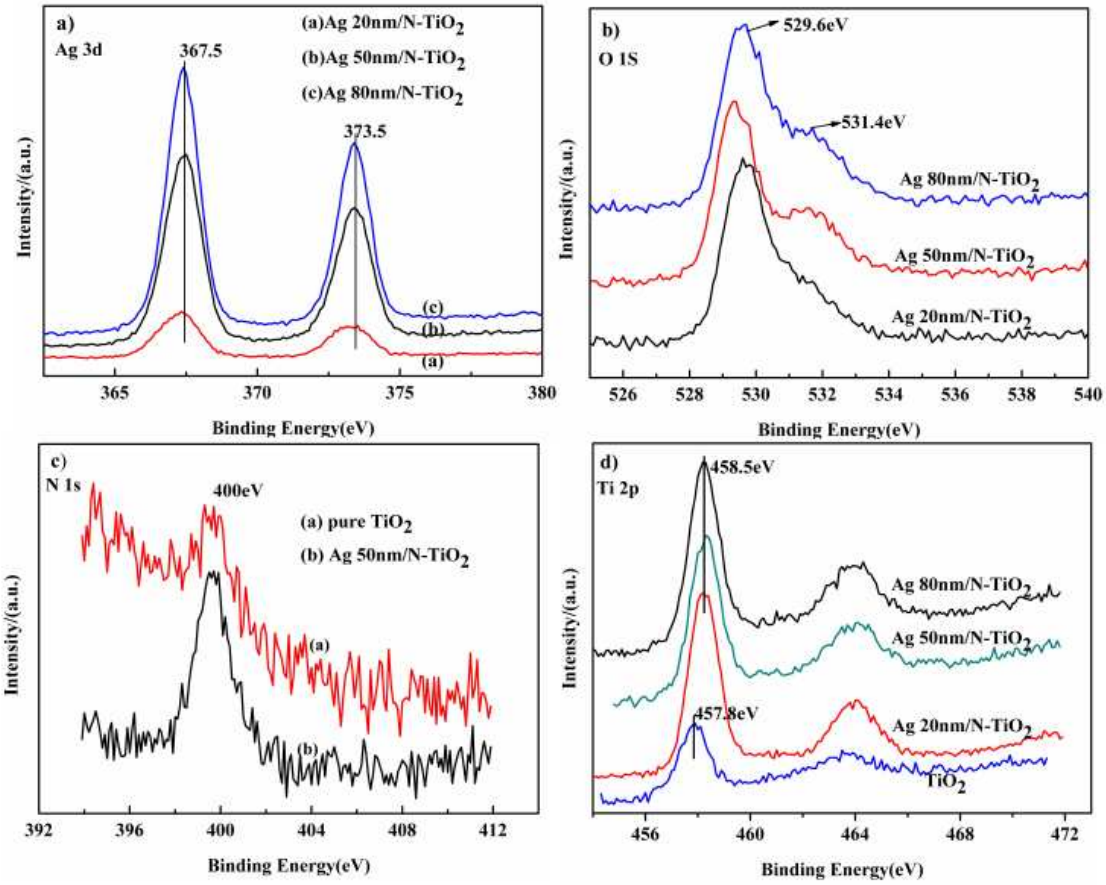

Figure 2. XPS spectra of the Ag/N-TiO_2 nanofilms; (a) Ag 3d, (b) O 1s, (c) N 1s, and (d) Ti 2p

It is known that nitrogen in TiO_2 plays a key role in changing the band gap, which determines the photocatalytic activity of TiO_2–based materials. Figure 2c shows the XPS spectrum of N 1s of pure TiO_2 and Ag 50nm/N-TiO_2 nanofilms. The intensity of N of the Ag 50nm/N-TiO_2 nanofilms is much stronger than that of the pure TiO_2, suggesting the presence of nitrogen with a binding energy of ca. 400 eV in the N-doped TiO_2 nanofilms. Nitrogen atoms occupy interstitial sites and form either Ti-N-O or Ti-O-N oxynitride bond. Figure 2d shows the Ti 2p spectrum of the Ag/N-TiO_2 nanofilms. The two peaks at 458.5 and 464.2 eV correspond to the binding energies of Ti $2p_{3/2}$ and Ti $2p_{1/2}$ levels, revealing the presence of the

Ti(IV) state. For the pure TiO_2 nanofilms, the peaks in the Ti 2p spectrum associated with the binding energies of Ti $2p_{3/2}$ and Ti $2p_{1/2}$ levels are at 457.8 and 463.5 eV [35], slightly less than the corresponding binding energies of the Ag/N-TiO_2 nanofilms, suggesting the presence of Ti(IV) state. This result confirms a lower electron density of the TiO_2 surface with the presence of Ag nanoparticles. There is a strong interaction between metallic Ag nanoparticles and TiO_2 in the Ag/TiO_2 nanofilms.

SEM and EDS analyses

Back-scattered electron (BSE) imaging was performed to identify the phases presented in the Ag/N-TiO_2 nanofilms. Figure 3 shows the BSE images, secondary electron (SEM) images, and the corresponding EDS spectrum of the Ag/N-TiO_2 nanofilms. The EDS patterns, as shown in Figure 3, display the peaks of Ti, O, Ag and N, confirming the presence of Ag and N elements in all the Ag/N-TiO_2 nanofilms.

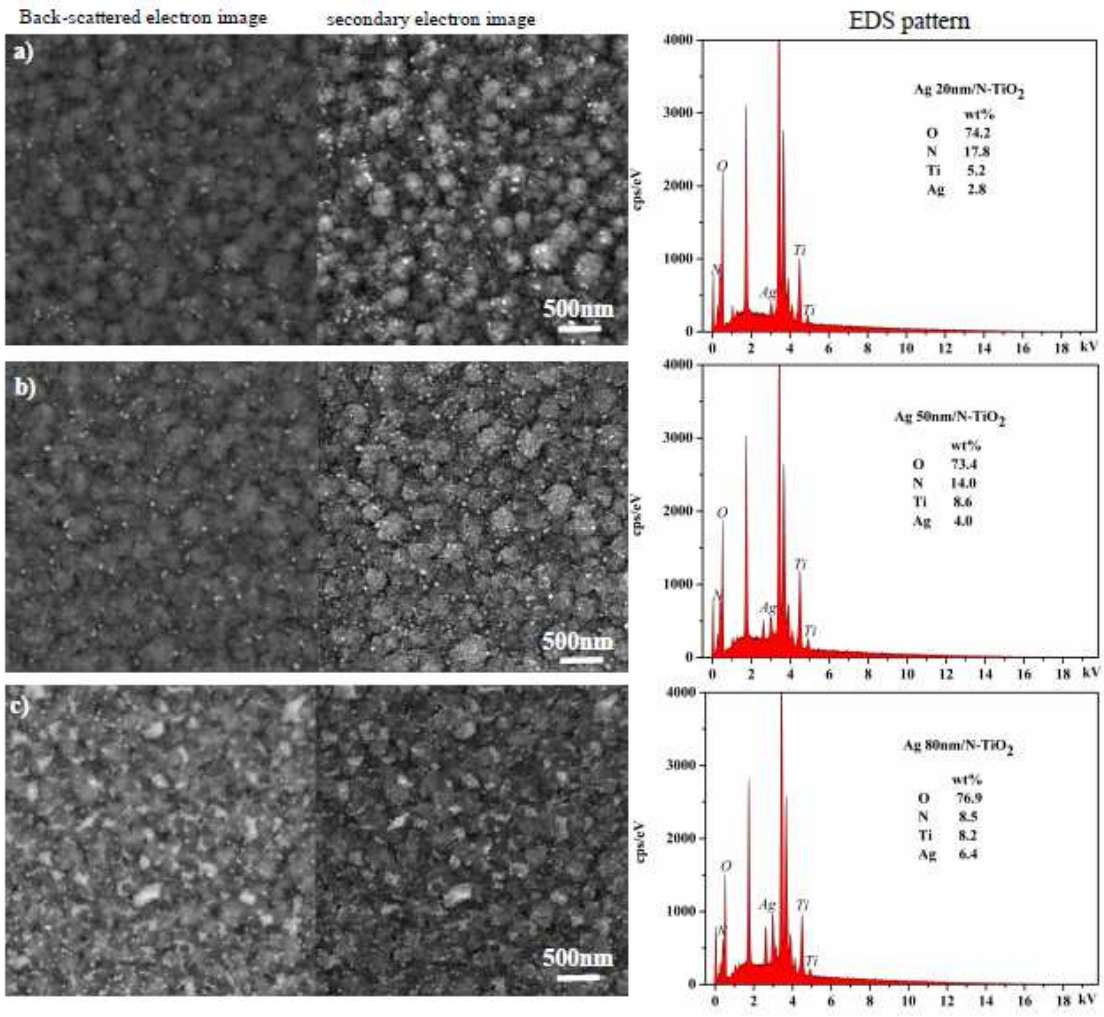

Figure 3. Back-scattered electron images, secondary electron images, and the corresponding EDS pattern of the Ag/N-TiO_2 nanofilms; (a) Ag 20nm/N-TiO_2, (b) Ag 50nm/N-TiO_2, and (c) Ag 80nm/N-TiO_2

In the BSE images, the white nanoparticles are Ag and the relatively dark nanoparticles are TiO_2. Ag nanoparticles are also present on the free surface of all the Ag/N-TiO_2 nanofilms, i.e. Ag atoms migrated through the TiO_2 nanofilm and moved from the Ag nanofilm between the glass substrate and the TiO_2 nanofilm to the free surface of the TiO_2 nanofilm. For the Ag 20 nm/N-TiO_2 nanofilms, the particle size of the Ag nanoparticles is in the range of 30-50 nm and the surface is relatively smooth. There is no observable difference of the particle sizes between the Ag 20nm/N-TiO_2 nanofilms and the Ag 50nm/N-TiO_2 nanofilms; while

increasing the fraction of Ag leads to the increase of the agglomerate of nanoparticles. The number of small Ag nanoparticles on the surface of the Ag 20nm/N-TiO_2 nanofilms is less than that on the surface of the Ag 50nm/N-TiO_2 nanofilms. Larger Ag nanoparticles are present on the surface of the Ag 80nm/N-TiO_2 nanofilms, which can become the recombination center of electrons and holes and become detrimental to the photocatalytic activity. It needs to control the sizes of Ag nanoparticles in order to limit the recombination of electrons and holes.

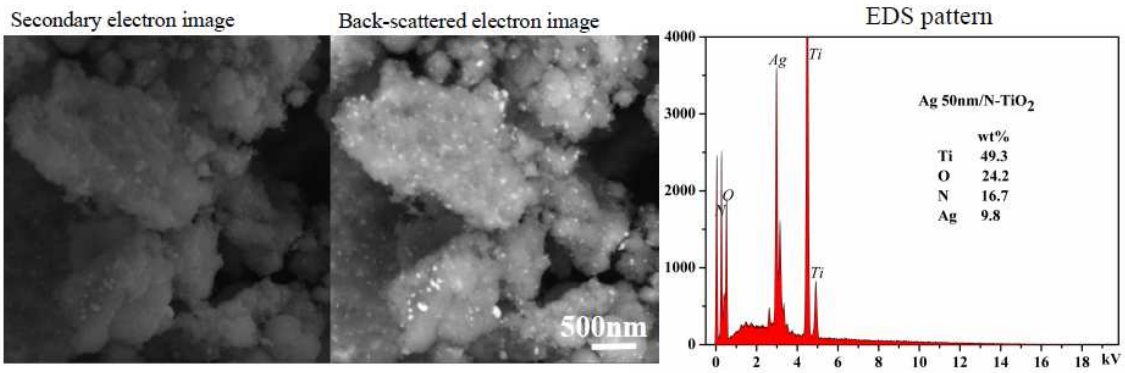

Figure 4. Back-scattered electron image, secondary electron image, and the corresponding EDS pattern of a scraped Ag 50nm/N-TiO_2 nanofilm after the heat treatment at 400 ^oC

Figure 4 shows the back-scattered electron image, secondary electron image, and the corresponding EDS pattern of a scraped Ag 50nm/N-TiO_2 nanofilm after the heat treatment at 400 ^oC. It is evident that Ag nanoparticles were well dispersed in the TiO_2 nanofilm, which qualitatively supports the observation that Ag nanoparticles are present on the free surface of all the Ag/N-TiO_2 nanofilms. The heat treatment causes the migration of Ag atoms through the TiO_2 nanofilm. The EDS pattern show the peaks of Ti, O, N and Ag elements, and no atoms from the glass substrates diffuse into the TiO_2 nanofilm during the heat treatment.

Okumu et al. [36] observed the formation of Ag nanoparticles in TiO_2 films from TiO_2/Ag/TiO_2 sandwiched structures, which were prepared by direct current magnetron sputtering. They suggested that the formation of Ag nanoparticles in TiO_2 films is controlled by the impinging, energetic oxygen ions formed during the sputtering of the second layer of TiO_2 and is driven by the Ag/TiO_2 interfacial energy. Okumu et al. [37] later suggested that the formation of Ag nanoparticles in TiO_2 films involves three steps, 1) the oxidation of Ag upon

reactive sputter deposition, 2) the dissociation of the oxide at high temperature, and 3) the formation of Ag nanoparticles by aggregation. However, they did not discuss the driving force for the migration of Ag atoms or Ag oxide in a TiO_2 film.

It is known that the diffusion flux of atoms or molecules is proportional to the gradient of chemical potential [38, 39]. The chemical potential consists of the contribution of the concentration of a substance, interfacial free energy and mismatch strain energy. The interfacial free energy is proportional to the interface area, and the mismatch strain energy is proportional to the volume of the material and the square of mismatch strain. During the magnetron sputtering, the mismatch strain can likely be introduced on the interface between the glass substrate and the Ag nanofilm and that between the Ag nanofilm and the TiO_2 nanofilm. The combination of the concentration gradient and the mismatch strain energy, if the contribution of the interfacial free energy is negligible, will cause the migration of Ag atoms from the Ag-rich region to the Ag-free region through the TiO_2 nanofilm. In addition, the TiO_2 nanofilm formed by the magnetron sputtering is amorphous. There are many open spaces, which allow the fast motion of Ag atoms and the nucleation and formation of Ag nanoparticles during heat treatment.

Photoluminescence (PL) analysis

It is known that the photoluminescence (PL) emission spectrum can be used to evaluate the efficiency of the trapping, migration, and transfer of charge carriers in order to understand the fate of electron-hole pairs in semiconductor particles [40, 41]. Figure 5 shows the TiO_2-based nanofilms, in which the Ag/N-TiO_2 nanofilms were calcined at 400 ^oC. The positions of the emission peaks of the Ag/N-TiO_2 nanofilms in the PL spectrum are similar to those of the TiO_2 nanofilms, while the emission intensity of the N-Ag/TiO_2 nanofilms is much smaller than that of the TiO_2 nanofilms. Such behavior indicates the efficient transfer of interfacial electrons from the conduction band of N-TiO_2 to the Ag nanoparticles, which act as electron sinks and suppress the recombination of photoinduced carriers [42]. From figure 5, one can note that the Ag 50nm/N-TiO_2 nanofilms have the lowest PL emission intensity. Thus, the electron-hole recombination rate in the Ag 50nm/N-TiO_2 nanofilms is the smallest, since the

recombination rate of the photoinduced electrons and holes is proportional to the emission intensity of photoluminescence.

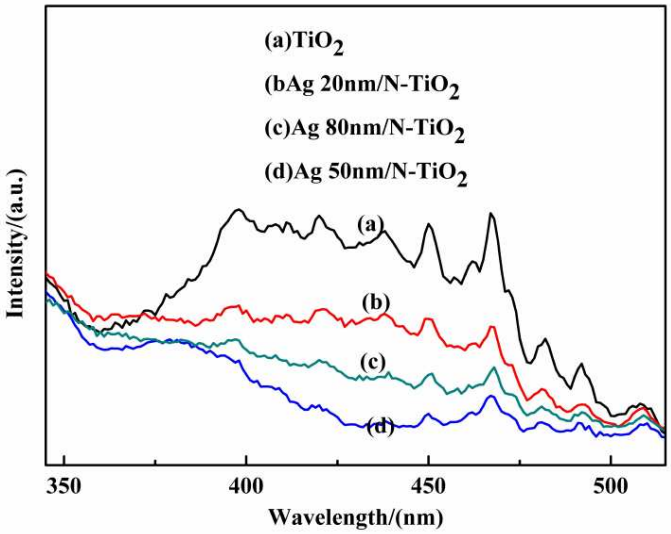

Figure 5. Photoluminescence emission spectra of TiO_2-based nanofilms (the Ag/N-TiO_2 nanofilms were calcined at 400 ^oC)

Optical properties of Ag/N-TiO_2 *nanofilms*

The UV-vis absorption of the TiO_2-based nanofilms was analyzed with a UV-Vis spectrophotometer (HITACHI: U-3900). Figure 6 shows the diffuse reflectance spectra of TiO_2 nanofilm, N-TiO_2 nanofilm, Ag/TiO_2 nanofilm, and Ag/N-TiO_2 nanofilms, in which all the materials were calcined at 400 ^oC. The small fluctuations of the absorption spectra is likely due to the interferences occurring at the interface of the thin film and the glass substrate, as discussed by Li et al. [43]. The pure TiO_2 nanofilms show the typical absorption of anatase with an intense transition in the UV region, which is due to the excitation of electrons from the valence band to the conduction band. The N-TiO_2 nanofilms possess both the enhanced UV and visible light absorption in comparison to the TiO_2 nanofilms. The cut off of the absorption edge is at ~375 nm (~3.3eV) for the TiO_2 nanofilms and ~410 nm (~3.1eV) for the N-TiO_2 nanofilms. There is a shift in the band gap of the N-TiO_2 nanofilms towards the visible spectrum, which can be attributed to the presence of nitrogen [44].

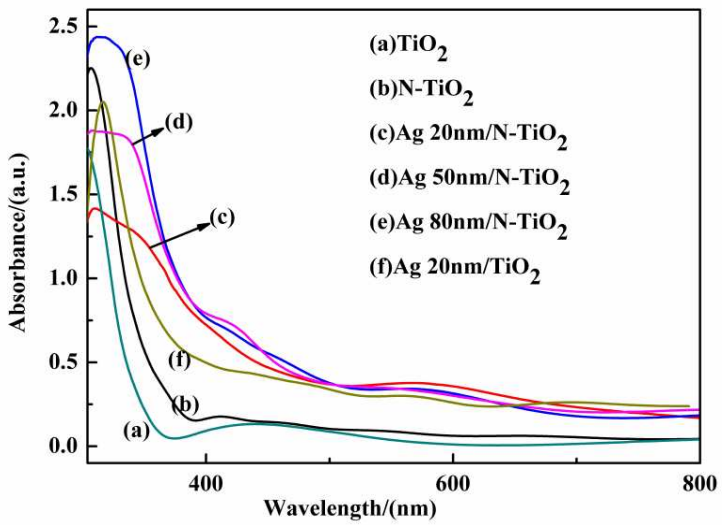

Figure 6. Diffuse reflectance spectra of TiO_2 nanofilms, N-TiO_2 nanofilms, Ag/TiO_2 nanofilms, and Ag/N-TiO_2 nanofilms (All the materials were calcined at 400 ^oC.)

Notably, all the Ag/N-TiO_2 nanofilms exhibit a broad absorption within the visible spectrum from 400 to 700 nm. Such behavior likely is due to the surface plasmon absorption (SPR) of Ag nanoparticles. The SPR of Ag nanoparticles extends the light absorption of the N-Ag/TO_2 nanofilms to larger wavelengths, increases the light scattering and activates photo-generated charge carriers through the transfer of plasmonic energy from Ag nanoparticles to the N-TiO_2 nanofilms [45].

In general, the doping of Ag in Ag-TiO_2 composites can cause a decrease of the band gap of TiO_2 due to the presence of localized energy levels [46], which allows the excitation of electrons of lower energies from the valence band to these energy levels instead of to the conduction band. The decrease of the band gap can improve the conversion efficiency of solar energy and assist the formation of reactive oxygen species under visible light irradiation [47]. From Figure 6, one can note that Ag/N-TiO_2 nanofilms exhibit more strong absorption of visible light than that of N-TiO_2 nanofilms, which confirme that nitrogen narrows the band gap of TiO_2. Such a decrease in the band gap likely will improve the photocatalytic efficiency. However, Ag nanoparticles as shown in Fig. 3 were formed inside and on the surface of the TiO_2 nanofilms. It is very difficult to ascertain the doping of Ag in TiO_2 nanofilms. The Ag nanoparticles likely act as electron scavengers to inhibit the motion of the electrons. It is

worth mentioning that the Ag 50nm/N-TiO_2 nanofilms exhibit strong light adsorption in both UV and visible light regions. The Ag 50nm/N-TiO_2 nanofilms likely will have better photocatalytic performance in both UV and visible light regions. Note that the Ag 50nm/N-TiO_2 nanofilms also exhibit more strong absorption at ~420 nm. The mechanism for such behavior is not clear, which might be due to the combination effect of the N doping and the localized surface plasma resonance (LSPR) from a large amount of Ag nanoparticles of small sizes, as suggested by Wu et al. [48].

As shown in figure 6, there is a broad absorption band at ~ 580 nm. There are reports on the broad absorption band in a range of 400-800 nm. Yang et al. [49] observed a broad absorption in the range of 490-800 nm with a summit at ~540 nm, and suggested that the LSPR effect of surface-deposited Ag(0) likely contributes to the enlargement of the optical absorption. They also suggested that the increase of the LSPR absorbance at ~540 nm is due to the increase of the Ag loading amount and aggregation degree. Wu et al. [48] observed a broad absorption ranging from 400 to 800 nm with a peak at about 425 nm and ascribed this phenomenon to the surface plasmon resonance (SPR) effect of Ag. In general, it is expected that the Ag nanoparticles on the free surface of TiO_2 films will introduce local SPR effect, leading to a broad absorption band in a range of 400-800 nm, as observed in this work. The wavelength of the broad absorption band might depend on the size and surface characteristics of Ag nanoparticles.

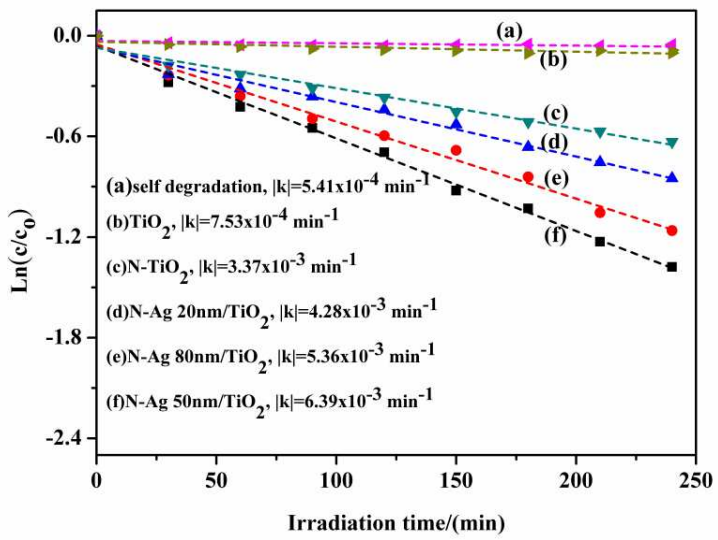

Figure 7. Temporal evolution of the concentration of the MB organic compound in aqueous solution with various TiO_2-based nanofilms under visible light irradiation (all the materials were calcined at 400 ^oC.)

Photocatalytic activity

The photocatalytic activity of the TiO_2-based nanofilms was investigated by measuring the degradation behavior of the MB organic compound in an aqueous solution under visible light irradiation. Figure 7 shows the temporal evolution of the normalized concentration of the MB organic compound in the aqueous solutions with various TiO_2-based nanofilms under visible light irradiation. Note that all the materials were calcined at 400 ^oC. In general, the use of TiO_2 nanofilms has improved the photo-degradation of the MB organic compound in the aqueous solution under visible light irradiation as a result of the photocatalytic effect of TiO_2 and the photosensitization of MB.

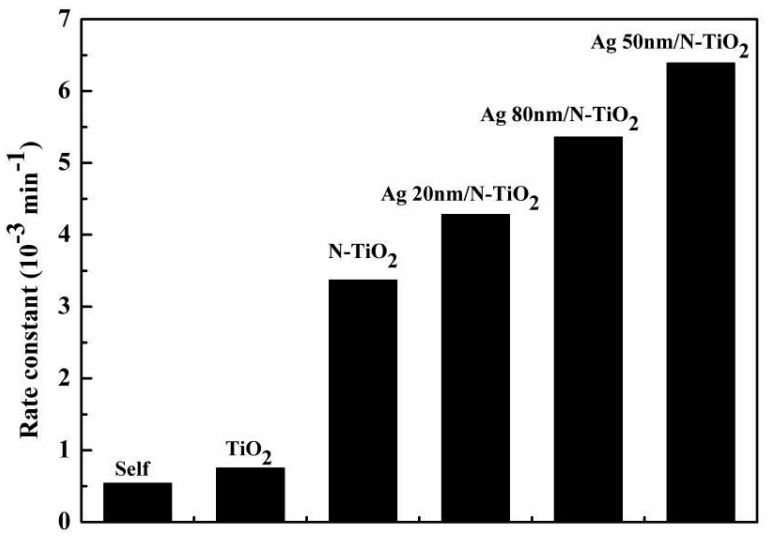

Figure 8. Rate constants in the unit of min^{-1} for the photo-induced degradation of MB in the aqueous solutions with different TiO_2-based nanofilms (all nanofilms were calcined at 400 ^oC.)

Under the experimental conditions, the temporal evolution of the concentration of the MB organic compound follows Eq. (2). The photo-induced degradation of MB is the first-order reaction. From the regression of experimental data, the rate constant, *k*, can be determined. Figure 8 shows the rate constants for the photo-induced degradation of MB in the aqueous solutions with different TiO_2-based nanofilms. It is evident that the rate constants for the aqueous solutions with N-TiO_2-based nanofilms are about one order larger than that of self-degradation and that with only pure TiO_2 nanofilms. The photocatalytic activities of N-TiO_2 nanofilms are improved due to the decrease of the band gap induced by nitrogen. However, the rate constants for the MB aqueous solutions with the Ag/N-TiO_2 nanofilms are larger than that with N-TiO_2 nanofilms, suggesting that silver further improves the photocatalytic activity of TiO_2 nanofilms possibly through the SPR effect of Ag nanoparticles which activates photo-generated charge carriers through the transfer of plasmonic energy. In addition, Ag can act as an e^- trap, reducing the recombination rate of h^+/e^- pairs, which favorites photocatalytic activity.

Xu et al. [50] studied the effect of particle size of TiO_2 on the photo-induced degradation of MB in a suspended aqueous solution and observed the increase of the adsorption rate and adsorbability of MB on suspended TiO_2 particles with the decrease of the particle sizes of TiO_2 particles. In studying the size effect of Ag nanoparticles on the plasmonic photocatalytic behavior of TiO_2 thin films with Ag nanoparticles embedded-SiO_2 films, Oh et al. [51] found that the TiO_2 films with a 7 nm-thick Ag film has the best decomposition rate. From Figure 8, one can note that the reaction constant for the photo-induced degradation of MB in the aqueous solution with Ag 80nm/N-TiO_2 nanofilms is less than that with Ag 50nm/N-TiO_2 nanofilms. Such a result reveals the size effect of Ag nanoparticles on the photo-induced degradation of MB, since larger Ag nanoparticles are present on the surface of the Ag 80nm/N-TiO_2 nanofilms, as shown in Figure 3c, than those on the surfaces of the Ag 20nm/N-TiO_2 and Ag 50nm/N-TiO_2 nanofilms. The larger Ag nanoparticles enhance the recombination rate of electrons and holes and lead to the decrease of the photocatalytic activity of Ag 80nm/N-TiO_2 nanofilms, which is qualitatively in accord with the size effect of Ag nanoparticles observed by Oh et al. [51].

To examine the stability of the TiO_2-based nanofilms in assisting the photodegradation of MB in the aqueous solutions under visible light irradiation, the TiO_2-based nanofilms were used repeatedly, and each cycle lasted 4 h. After each cycle, the residual concentration of MB was measured at a wavelength of 664 nm, using an UV/VIS spectrophotometer (Perkin-Elmer, Lambda 35). Before starting each new cycle, the remaining solution was replaced with fresh aqueous MB solution (5 $mg \cdot L^{-1}$) of 50 ml.

Define the degradation rate of the TiO_2-based nanofilms as $(1-c_f)/c_0$, in which c_f is the residual concentration of MB after the test. Figure 9 shows the variation of the degradation rate with the number of cycles. The degradation rate decreases with the number of cycles, suggesting that efficiency of the TiO_2-assisted photodegradation of MB decreases with time likely due to the interaction between the MB aqueous solution and the surface of the TiO_2 nanofilms. Significant drop of the photodegradation of MB in the MB aqueous solution with the TiO_2 nanofilms after 4 cycles is observed. The degradation rates of the N-TiO_2 nanofilms, Ag 50nm/N-TiO_2 nanofilms, and Ag 50nm/TiO_2 nanofilms in the aqueous solutions of MB

are much larger than that of the TiO_2 nanofilms; and the Ag 50nm/N-TiO_2 nanofilms have the largest degradation rate.

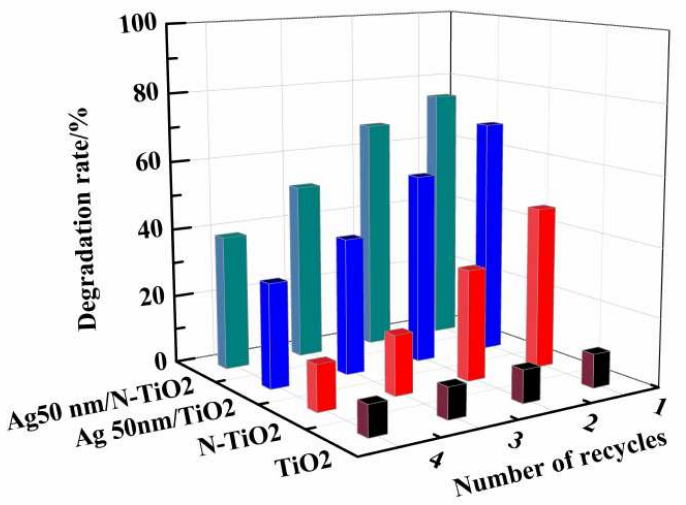

Figure 9. Dependence of the degradation rate of the TiO_2-based nanofilms on the number of cycles for the photodegradation of MB (all nanofilms were calcined at 400 ^oC.)

Table 1. Rate constants for the photo-induced degradation of MB in the aqueous solutions with different TiO_2-based nanofilms for different cycles

	Rate constant (k) (min^{-1})			
Number of cycles	N-Ag 50nm/TiO_2	Ag 50nm/TiO_2	N-TiO_2	TiO_2
1	6.39×10^{-3}	4.16×10^{-3}	3.37×10^{-3}	7.53×10^{-4}
2	5.12×10^{-3}	3.84×10^{-3}	2.86×10^{-3}	7.53×10^{-4}
3	3.91×10^{-3}	2.69×10^{-3}	1.85×10^{-3}	6.87×10^{-4}
4	2.66×10^{-3}	2.53×10^{-3}	1.63×10^{-3}	4.60×10^{-4}

Table 1 lists the rate constants for the photo-induced degradation of MB in the aqueous solutions with different TiO_2-based nanofilms for different cycles. The rate constants decrease with increasing the number of cycles, qualitatively in accord with the behavior of the degradation rate of the TiO_2-based nanofilms in assisting the potodegradation of the MB

aqueous solutions. However, the Ag 50nm/N-TiO_2 nanofilms still have the largest rate constant for the photo-induced degradation of MB in the aqueous solution in the 4th cycle.

It is known that TiO_2 is an N-type semiconductor. The reaction in the aqueous solution of MB under visible light irradiation involves the excitation of electrons from MB molecules adsorbed on the surface of the TiO_2 nanofilms from the valence band into the conduction band of TiO_2 semiconductor [52, 53]. The transferred electrons, which can be trapped subsequently by molecular oxygen and adsorbed on the surface of the TiO_2 film, form $O^{\cdot -}$ to generate highly active $^{\cdot}$OOH and $^{\cdot}$OH radicals. The reaction of the $^{\cdot}$OOH and $^{\cdot}$OH radicals with the radical cation of MB leads to the formation of intermediates or completely mineralized product and the decomposition of MB. The results shown in Figure 9 and Table 1 imply that there exist significantly irreversible reactions on the surface of the TiO_2 nanofilms, which reduces the number of the excited electrons from MB molecules adsorbed on the surface of the TiO_2 nanofilms, which jump from the valence band into the conduction band of TiO_2 semiconductor. The synergistic effect of N and Ag inhibits the irreversible reactions on the surface of the TiO_2 nanofilms, and there is much less decrease in the number of the excited electrons from MB molecules adsorbed on the surface of the Ag 50nm/N-TiO_2 nanofilms, jumping from the valence band into the conduction band of TiO_2 semiconductor, than that on the surface of the TiO_2 nanofilms.

4. Summary

Pure TiO_2 nanofilms and Ag/TiO_2 bilayer nanofilms with N were deposited on glass substrates by magnetron sputtering. The heat treatment of the Ag/N-TiO_2 nanofilms at 400 ^{o}C led to the formation of Ag nanoparticles, which were dispersed inside the TiO_2 nanofilms as well as on the free surface of the TiO_2 nanofilms. The XRD patterns reveal that only the anatase phase in the N-Ag/TiO_2 nanofilms was formed at 400 ^{o}C . The XPS analysis suggests that there are the migration of electrons from TiO_2 nanofilms to metallic Ag nanoparticles and a strong interaction between Ag nanostructures and TiO_2 nanofilms at the interface of the nano-heterostructures. Nitrogen reduces the electron-hole recombination rate in the Ag/N-TiO_2 nanofilms, which improves the photocatalytic activity of TiO_2 nanofilms. The rate constants for the aqueous solutions of MB with N-TiO_2-based nanofilms are about one order

larger than that of self-degradation and that with only pure TiO_2 nanofilms. The photocatalytic activities of N-TiO_2 and Ag/N-TiO_2 nanofilms are improved due to the decrease of the band gap induced by nitrogen and the immobilization of electrons by Ag nanoparticles. The rate constants for the MB aqueous solutions with the Ag/N-TiO_2 nanofilms are larger than that with N-TiO_2 nanofilms, suggesting that Ag nanoparticles further improve the photocatalytic activity of TiO_2 nanofilms possibly through the SPR effect of Ag nanoparticles which activates photo-generated charge carriers through the transfer of plasmonic energy.

Acknowledgment

LW is grateful for the financial support from the National Natural Science Foundation of China (51301118, 51175363) and the Scientific and Technological Innovation Programs of Higher Education Institutions in Shanxi province (2013108). FY is grateful for the support from the "Hundred-People-Plan" Program of Shanxi (2014).

References:

1. X. M. Chen, Z. J. Liu, J. T. Tang, C. L. Teng, T. J. Cai and Q. Deng, *Journal of Porous Materials*, 2015, **22**, 361-367.
2. L. J. Chen, J. T. Tian, H. Qiu, Y. S. Yin, X. Wang, J. H. Dai, P. W. Wu, A. P. Wang and L. Chu, *Ceramics International*, 2009, **35**, 3275-3280.
3. L. Rizzo, J. Koch, V. Belgiorno and M. A. Anderson, *Desalination*, 2007, **211**, 1-9.
4. Y. J. Zhang and J. N. Shen, *Rare Metal Materials and Engineering*, 2006, **35**, 92-95.
5. W. Y. Chen, Y. B. Liu, Y. Ma and W. X. Yang, *Journal of Power Sources*, 2015, **273**, 1127-1135.
6. G. Jeong, J. G. Kim, M. S. Park, M. Seo, S. M. Hwang, Y. U. Kim, Y. J. Kim, J. H. Kim and S. X. Dou, *Acs Nano*, 2014, **8**, 2977-2985.
7. L. Bai, F. Fang, Y. Y. Zhao, Y. G. Liu, J. P. Li, G. Y. Huang and H. Y. Sun, *Rsc Advances*, 2014, **4**, 43039-43046.
8. Q. L. Wu, J. C. Li, R. D. Deshpande, N. Subramanian, S. E. Rankin, F. Q. Yang and Y. T. Cheng, *Journal of Physical Chemistry C*, 2012, **116**, 18669-18677.
9. D. P. Wu, S. Zhang, S. W. Jiang, J. J. He and K. Jiang, *Journal of Alloys and Compounds*, 2015, **624**, 94-99.
10. G. X. Wang, X. J. Zhu and J. G. Yu, *Journal of Power Sources*, 2015, **278**, 344-351.
11. C. L. Wang, J. Y. Liao, Y. B. Zhao and A. Manthiram, *Chemical Communications*, 2015, **51**, 2848-2850.
12. L. L. Jiang, X. Lu, C. M. Xie, G. J. Wan, H. P. Zhang and Y. H. Tang, *Journal of Physical Chemistry C*, 2015, **119**, 3903-3910.
13. M. R. Dhananjeyan, J. Kiwi and K. R. Thampi, *Chemical Communications*, 2000, **10**, 1443-1444.
14. I. K. Konstantinou and T. A. Albanis, *Applied Catalysis B-Environmental*, 2004, **49**, 1-14.
15. V. Scuderi, G. Impellizzeri, L. Romano, M. Scuderi, M. V. Brundo, K. Bergum, M. Zimbone, R. Sanz, M. A. Buccheri, F. Simone, G. Nicotra, B. G. Svensson, M. G. Grimaldi and V. Privitera, *Nanoscale*, 2014, **6**, 11189-11195.

16. E. Hendry, M. Koeberg, B. O'Regan and M. Bonn, *Nano Letters*, 2006, **6**, 755-759.
17. A. L. Linsebigler, G. Q. Lu and J. T. Yates, *Chemical Reviews*, 1995, **95**, 735-758.
18. P. Salvador, *Journal of Applied Physics*, 1984, **55**, 2977-2985.
19. Y. J. Hwang, C. Hahn, B. Liu and P. D. Yang, *Acs Nano*, 2012, **6**, 5060-5069.
20. A. Tanaka, S. Sakaguchi, K. Hashimoto and H. Kominami, *Acs Catalysis*, 2013, **3**, 79-85.
21. Z. T. Li, Z. Y. Ren, Y. Qu, S. C. Du, J. Wu, L. J. Kong, G. H. Tian, W. Zhou and H. G. Fu, *European Journal of Inorganic Chemistry*, 2014, **2014**, 2146-2152.
22. D. M. Chen, Z. Y. Jiang, J. Q. Geng, Q. Wang and D. Yang, *Industrial & Engineering Chemistry Research*, 2007, **46**, 2741-2746.
23. R. Asahi, T. Morikawa, T. Ohwaki, K. Aoki and Y. Taga, *Science*, 2001, **293**, 269-271.
24. D. Kannaiyan, M. A. Cha, Y. H. Jang, B. H. Sohn, J. Huh, C. Park and D. H. Kim, *New Journal of Chemistry*, 2009, **33**, 2431-2436.
25. J. X. Xu, X. H. Xiao, A. L. Stepanov, F. Ren, W. Wu, G. X. Cai, S. F. Zhang, Z. G. Dai, F. Mei and C. Z. Jiang, *Nanoscale Research Letters*, 2013, **8**, 1-5.
26. K. S. Yang, Y. Dai and B. B. Huang, *Journal of Physical Chemistry C*, 2007, **111**, 12086-12090.
27. G. H. Tian, Y. J. Chen, K. Pan, D. J. Wang, W. Zhou, Z. Y. Ren and H. G. Fu, *Applied Surface Science*, 2010, **256**, 3740-3745.
28. D. L. Shieh, Y. S. Lin, J. H. Yeh, S. C. Chen, B. C. Lin and J. L. Lin, *Chemical Communications*, 2012, **48**, 2528-2530.
29. J. C. S. Wu and C. H. Chen, *Journal of Photochemistry and Photobiology a-Chemistry*, 2004, **163**, 509-515.
30. S. P. Lim, A. Pandikumar, N. M. Huang and H. N. Lim, *RSC Advances*, 2014, **4**, 38111-38118.
31. S. P. Lim, A. Pandikumar, N. M. Huang and H. N. Lim, *International Journal of Hydrogen Energy*, 2014, **39**, 14720-14729.
32. P. Gorska, A. Zaleska, E. Kowalska, T. Klimczuk, J. W. Sobczak, E. Skwarek, W. Janusz and J. Hupka, *Applied Catalysis B-Environmental*, 2008, **84**, 440-447.

33. L. Zhao, L. Z. Fan, M. Q. Zhou, H. Guan, S. Y. Qiao, M. Antonietti and M. M. Titirici, *Advanced Materials*, 2010, **22**, 5202-5206.
34. H. W. Chen, Y. Ku and Y. L. Kuo, *Chemical Engineering & Technology*, 2007, **30**, 1242-1247.
35. Y. M. Liu, W. G. Zhang, L. P. Bian, W. Liang, J. J. Zhang and B. Yu, *Materials Science in Semiconductor Processing*, 2014, **21**, 26-32.
36. J. Okumu, C. Dahmen, A. N. Sprafke, M. Luysberg, G. von Plessen and M. Wuttig, *Journal of Applied Physics*, 2005, **97**, 094305.
37. J. Okumu, D. Kohl, A. Sprafke, G. von Plessen and M. Wuttig, *Journal of Applied Physics*, 2010, **108**, 063529.
38. F. Q. Yang, *Materials Science and Engineering a-Structural Materials Properties Microstructure and Processing*, 2005, **409**, 153-159.
39. F. Q. Yang, *Science China-Physics Mechanics & Astronomy*, 2012, **55**, 955-962.
40. Y. Bai, P. Q. Wang, J. Y. Liu and X. J. Liu, *Rsc Advances*, 2014, **4**, 19456-19461.
41. F. B. Li and X. Z. Li, *Chemosphere*, 2002, **48**, 1103-1111.
42. X. J. Bai, R. L. Zong, C. X. Li, D. Liu, Y. F. Liu and Y. F. Zhu, *Applied Catalysis B-Environmental*, 2014, **147**, 82-91.
43. Q. Li, W. Liang and J. K. Shang, *Appl Phys Lett*, 2007, **90**, 063109.
44. N. S. Chaudhari, S. S. Warule, S. A. Dhanmane, M. V. Kulkarni, M. Valant and B. B. Kale, *Nanoscale*, 2013, **5**, 9383-9390.
45. S. Linic, P. Christopher and D. B. Ingram, *Nature Materials*, 2011, **10**, 911-921.
46. E. P. Melian, O. G. Diaz, J. M. D. Rodriguez, G. Colon, J. A. Navio, M. Macias and J. P. Pena, *Applied Catalysis B-Environmental*, 2012, **127**, 112-120.
47. M. Pelaez, N. T. Nolan, S. C. Pillai, M. K. Seery, P. Falaras, A. G. Kontos, P. S. M. Dunlop, J. W. J. Hamilton, J. A. Byrne, K. O'Shea, M. H. Entezari and D. D. Dionysiou, *Applied Catalysis B-Environmental*, 2012, **125**, 331-349.
48. T. S. Wu, K. X. Wang, G. D. Li, S. Y. Sun, J. Sun and J. S. Chen, *Acs Appl Mater Inter*, 2010, **2**, 544-550.
49. L. B. Yang, X. Jiang, W. D. Ruan, J. X. Yang, B. Zhao, W. Q. Xu and J. R. Lombardi, *J*

Phys Chem C, 2009, **113**, 16226-16231.

50. N. P. Xu, Z. F. Shi, Y. Q. Fan, J. H. Dong, J. Shi and M. Z. C. Hu, *Industrial & Engineering Chemistry Research*, 1999, **38**, 373-379.
51. J. H. Oh, H. Lee, D. Kim and T. Y. Seong, *Surface & Coatings Technology*, 2011, **206**, 185-189.
52. K. R. Gopidas and P. V. Kamat, *Journal of Physical Chemistry*, 1989, **93**, 6428-6433.
53. K. Vinodgopal and P. V. Kamat, *Journal of Physical Chemistry*, 1992, **96**, 5053-5059.